ABCA4-Associated Retinal Degenerations Spare Structure and Function of the Human Parapapillary Retina

Artur V. Cideciyan,[1] *Malgorzata Swider,*[1] *Tomas S. Aleman,*[1] *Alexander Sumaroka,*[1] *Sharon B. Schwartz,*[1] *Marisa I. Roman,*[1] *Ann H. Milam,*[1] *Jean Bennett,*[1] *Edwin M. Stone,*[2] *and Samuel G. Jacobson*[1]

Purpose. To study the parapapillary retinal region in patients with *ABCA4*-associated retinal degenerations.

Methods. Patients with Stargardt disease or cone–rod dystrophy and disease-causing variants in the *ABCA4* gene were included. Fixation location was determined under fundus visualization, and central cone-mediated vision was measured. Intensity and texture abnormalities of autofluorescence (AF) images were quantified. Parapapillary retina of an eye donor with ungenotyped Stargardt disease was examined microscopically.

Results. AF images ranged from normal, to spatially homogenous abnormal increase of intensity, to a spatially heterogenous speckled pattern, to variably sized patches of low intensity. A parapapillary ring of normal-appearing AF was visible at all disease stages. Quantitative analysis of the intensity and texture properties of AF images showed the preserved region to be an annulus, at least 0.6 mm wide, surrounding the optic nerve head. A similar region of relatively preserved photoreceptor nuclei was apparent in the donor retina. In patients with foveal fixation, there was better cone sensitivity at a parapapillary locus in the nasal retina than at the same eccentricity in the temporal retina. In patients with eccentric fixation, ~30% had a preferred retinal locus in the parapapillary retina.

Conclusions. Human retinal degenerations caused by *ABCA4* mutations spare the structure of retina and RPE in a circular parapapillary region that commonly serves as the preferred fixation locus when central vision is lost. The retina between fovea and optic nerve head could serve as a convenient, accessible, and informative region for structural and functional studies to determine natural history or outcome of therapy in *ABCA4*-associated disease. (*Invest Ophthalmol Vis Sci.* 2005; 46:4739–4746) DOI:10.1167/iovs.05-0805

From the [1]Scheie Eye Institute, Department of Ophthalmology, University of Pennsylvania, Philadelphia, Pennsylvania; the [2]Howard Hughes Medical Institute and Department of Ophthalmology, University of Iowa Hospitals and Clinics, Iowa City, Iowa.

Supported by National Institutes of Health Grants EY-13385, -13729, -10820,-12156; Macula Vision Research Foundation; Foundation Fighting Blindness, Inc.; The Macular Disease Foundation; F. M. Kirby Foundation; Sam B. Williams Fund; and The Paul and Evanina Bell Mackall Foundation Trust.

Submitted for publication June 24, 2005; revised August 2, 2005; accepted September 28, 2005.

Disclosure: **A.V. Cideciyan**, None; **M. Swider**, None; **T.S. Aleman**, None; **A. Sumaroka**, None; **S.B. Schwartz**, None; **M.I. Roman**, None; **A.H. Milam**, None; **J. Bennett**, None; **E.M. Stone**, None; **S.G. Jacobson**, None

The publication costs of this article were defrayed in part by page charge payment. This article must therefore be marked "*advertisement*" in accordance with 18 U.S.C. §1734 solely to indicate this fact.

Corresponding author: Artur V. Cideciyan, Scheie Eye Institute, University of Pennsylvania, 51 North 39th Street, Philadelphia, PA 19104; cideciya@mail.med.upenn.edu.

The *ABCA4* gene encodes the ABCR protein (also known as Rim protein) localized to rod and cone photoreceptor outer segments.[1–5] Evidence to date supports the involvement of ABCR in the active transport of a complex of all-*trans*-retinal and phosphatidylethanolamine.[6–8] Mutations in *ABCA4* cause autosomal recessive forms of retinal degeneration (RD) that are associated with varied fundus appearance, wide-ranging disease severity, and a diverse set of clinical diagnoses.[9–17] The single common phenotypic feature reported in patients with *ABCA4*-associated RD (*ABCA4*-RD) is the involvement of the macula,[2,9–17] with very rare exceptions.[13]

The detailed natural history of spatio-temporal disease progression in *ABCA4*-RD is not known. Based on the predominant involvement of the macula in *ABCA4*-RD and effects on the peripheral retina in a subset of those patients, it is parsimonious to hypothesize a generalized central to peripheral (centrifugal) expansion of the retinal degeneration with age in most patients. Studies in Stargardt disease (STGD) of unknown genotype have commonly provided evidence for a centrifugal expansion of the degeneration[18–21] sometimes sparing the fovea or the foveola.[21–23] Stages of *ABCA4*-RD disease observed in cross-sectional studies have been generally consistent with the centrifugal expansion hypothesis.[11,15–17] Some reports in STGD, however, have shown a retinal region encircling the optic nerve that may be protected from retinal degeneration and forms an island of exception to the centrifugal expansion hypothesis.[20,24–28] In the current work, we used autofluorescence (AF) imaging in the vicinity of the parapapillary retina to examine whether, and under what conditions, this region is spared from retinal degeneration in *ABCA4*-RD, and whether such sparing has implications for visual function.

Methods

Patients

The study population was a subset (n = 41; those who had fixation testing) of patients recently reported.[16] They had clinical diagnoses of STGD[11] or cone–rod dystrophy (CRD)[15] and one or more changes in the *ABCA4* gene considered to be disease-causing variants. The patient numbers in the current work refer exactly to those in the previous publication.[16] Research procedures were in accordance with institutional guidelines and the Declaration of Helsinki. All patients gave written informed consent.

Visual Function Studies

A complete eye examination was performed in all subjects including Goldmann kinetic perimetry with V-4e and I-4e targets. The preferred locus of fixation was determined with optical coherence tomography (OCT; Carl Zeiss Meditec, Dublin, CA). Specifically, after alignment of the eye with the OCT instrument, patients were asked to fixate the "landmark" spot (a bright red light) and a 4.5-mm-long scan was moved until the cross-section of the anatomic fovea could be identified at the center of the scan. Then, an OCT scan and a corresponding fundus image were obtained for documentation, and fixation location was quantified with respect to the location of the anatomic fovea.

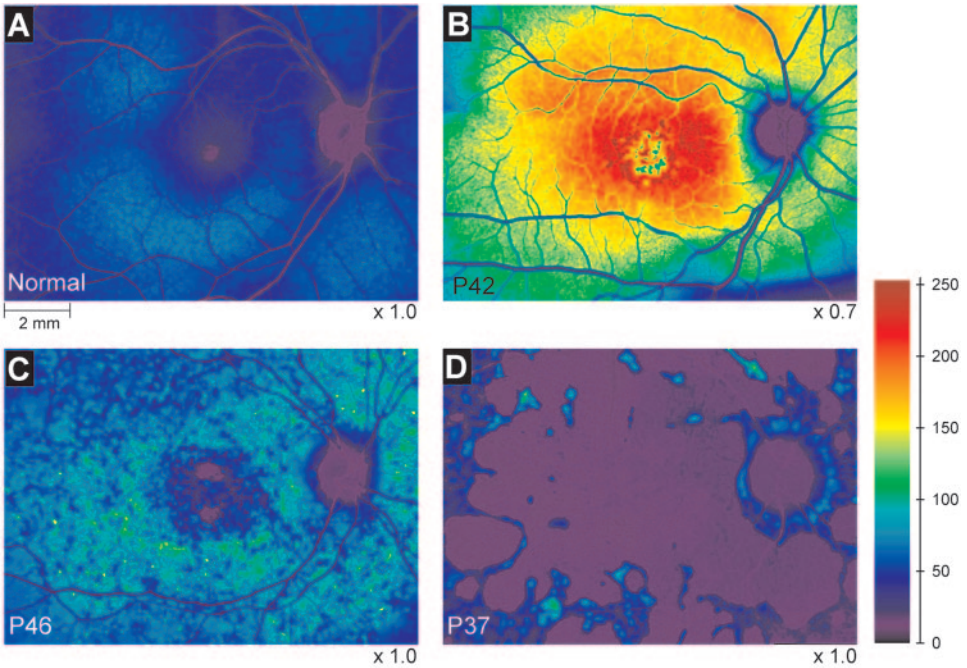

FIGURE 1. Standardized images of AF in a representative normal subject (**A**) and three patients (**B–D**) with *ABCA4*-RD. Excitation wavelength, 488 nm. Intensities were mapped to the pseudocolor scale shown. Results of P42 were uniformly scaled (×0.7) to fit the 256-level dynamic range. *Black*: no image data; *purple*: the dark level of the detector. All eyes are shown as equivalent right eyes.

In all patients with documented stable fixation at the anatomic fovea, horizontal profiles of cone sensitivity were obtained with orange (600 nm; 200 ms; 1.7 ° diameter) stimuli presented on a white (2.7 log phot-td) background on a modified[29] computerized static perimeter (HFA; Carl Zeiss Meditec, Inc.).

AF Imaging and Analyses

Imaging was done with a confocal scanning laser ophthalmoscope (HRA; Heidelberg Engineering, Dossenheim, Germany), as previously described.[16] AF images were obtained with 488-nm excitation and >500-nm emission. All images were acquired with a lateral magnification wherein a 30° × 30°-square field was sampled onto 512 × 512 pixels. Custom-written software (MatLab 6.5; The MathWorks, Natick, MA) was used, first to transform each file containing series of consecutive images of AF intensity into a stack of 8-bit raw images. Frames with blinks or midframe eye movements were discarded, and the remaining frames were spatially transformed to correct for imaging-system derived distortions. This corrected stack was loaded into an image-processing program (ImageJ, ver 1.34n; http://rsb.info.nih.gov/ij; developed by Wayne Rasband and provided in the public domain by the National Institutes of Health, Bethesda, MD). The images in the stack were automatically registered by using a pair of programs (turboreg and stackreg[30]; http://bigwww.epfl.ch/algorithms.html/ provided in the public domain by the Bioimaging Group; École Polytechnique Féderale de Lausanne, Lausanne, Switzerland). The mean AF intensity was calculated at each pixel after registration. A wide-field image montage was assembled from six to eight images by manually specifying retinal landmark pairs corresponding to each other in overlapping segments using custom-written software (MatLab 6.5; The MathWorks). Images from left eyes were transformed into equivalent right eyes and further transformed to register the anatomic fovea and the center of the optic nerve head (ONH) to predetermined locations based on mean normal results. The intensity of each image was normalized by the mean intensity at the center of the ONH. The resulting intensities were mapped to a custom pseudocolor scale which was slightly modified from a previously published version.[16]

To quantify the local heterogeneity of the AF intensity, run-length[31–33] was calculated for a fixed criterion in eight principal directions for each pixel. The mean run-length of a pixel represents the size of a local region showing homogeneity of intensity. Further details of this method are in the Appendix. All intensity and run-length images were transformed into pseudoprofiles by using semipolar integral analysis in the neighborhood of the ONH. Further details of this method are in the Appendix.

Histopathology

A sample of the right retina of a previously published[34] donor eye (Foundation Fighting Blindness, FFB#219) was available for study. In brief, the patient was a 62-year-old woman who had died of lung cancer. At the time of death, the donor had advanced macular degeneration from STGD but without a known molecular cause. The eye was enucleated at 4 hours and 20 minutes after death and was slit at the pars plana. Ten minutes later, it was placed into fixative.[34] The tissue sample containing the nasal half of the ONH was embedded without osmication in glycol methacrylate (JB-4; Polysciences, Wilmington, DE), sectioned at 2 μm, and stained with Richardson's methylene blue/azure II mixture. Sections were examined with a microscope (Leica DMR, Deerfield, IL) and photographed (EliteChrome ASA 400 film; Eastman Kodak, Rochester, NY) with a calibration slide.

RESULTS

Accumulated lipofuscin in RPE cells is the dominant fluorophore that contributes to the topographic variation of AF intensity across the human retina on excitation with short-wavelength light.[16,35–40] Features of AF intensity distribution across the central retina in normal eyes have been described.[39,41] A representative normal subject shows a deep trough of AF signal at the fovea (Fig. 1), corresponding to the absorption of the excitation light by macular pigment; and there is loss of signal at the retinal blood vessels corresponding to the absorption by blood. The AF signal originating from the normal ONH is below the level of detection. The peak of AF intensity forms an approximate circle at an eccentricity of ~3 mm corresponding to the highest density of rod photoreceptors in the human retina.[35,41,42]

An early sign of *ABCA4*-disease that is detectable noninvasively is the abnormality of AF intensity.[14,16,28,43,44] Illustrating an early *ABCA4*-disease stage is Patient 42 (P42, see Ref. 16), a 23-year-old man with clinically diagnosed[11] STGD phenotype I and a molecularly diagnosed G1961E mutation in the *ABCA4* gene. He had best corrected visual acuities of 20/40 and 20/100 in the right and left eyes, respectively. Both eyes showed

a full extent of Goldmann kinetic visual field with the V-4e and I-4e test targets but a relative central scotoma with the I-4e target. AF imaging of his left eye showed a dramatic increase of intensity across the central retina (Fig. 1B, displayed as equivalent right eye). The abnormal intensity was spatially homogeneous throughout most of the central retina except near the fovea where there were small regions of AF intensity loss with the resultant local spatial heterogeneity. Notable was a region of normal-appearing AF intensity encircling the ONH. A more advanced disease stage of *ABCA4*-RD is illustrated by P46, a 48-year-old woman with clinically diagnosed STGD phenotype II and a molecularly diagnosed R2030Q mutation in the *ABCA4* gene. She had best corrected visual acuities of 20/200 and 20/20 in the right and left eyes, respectively, and full peripheral extent of kinetic fields. Centrally, there was a small island of retained function (with the V-4e target) surrounded by an absolute scotoma and a larger relative scotoma. AF imaging of her right eye showed intensities distributed mostly within the normal range, but there was abnormal spatial heterogeneity (Fig. 1C) with a speckled pattern. This pattern has been hypothesized to correspond to microscopic variation in the rates of abnormal lipofuscin accumulation, or to the patchy loss of a subset of RPE cells, or to the reduction of OS shedding as the overlying retina degenerates.[16] Two regions of presumed RPE atrophy were also apparent as patches of low intensity in the superior and inferior parafovea. Of note, there was a spatially homogenous circular region of normal-appearing intensity at the parapapillary retina. A severe disease stage of *ABCA4*-RD is represented by P37, a 41-year-old man with clinically diagnosed STGD phenotype II and a molecularly diagnosed IVS40+5G→A mutation in the *ABCA4* gene. He had best corrected visual acuities of 20/400 and 20/200 in right and left eyes, respectively. Kinetic perimetry with the V-4e target showed superior field limitation but was otherwise full in peripheral extent; an absolute central scotoma was present in each eye. There was no detection of the I-4e target. AF imaging of his right eye showed extensive regions of presumed RPE atrophy across the posterior pole, with small intervening regions of detectable AF probably originating from retained RPE. A normal-appearing parapapillary ring was visible (Fig. 1D).

To confirm and extend the visual impressions of parapapillary preservation, we quantified AF results in *ABCA4*-RD patients and compared them to a group of normal subjects. Distribution of lipofuscin accumulation was estimated from AF intensities. Spatial heterogeneity of lipofuscin accumulation was derived using run-length analysis where mean run-length of a pixel represents the size of a local region showing homogeneity of intensity. Intensity and run-length images centered on the ONH were vertically bisected to form nasal and temporal halves, transformed from rectangular to polar coordinates, and integrated along the angular dimension to produce pseudoprofiles. Data from four patients overlaid on normal limits represent the spectrum of results observed (Fig. 2). P20 had a normal parapapillary region and surrounding area; both the intensity and the local homogeneity of the AF imaging within 2.5 mm of the center of the ONH fell within or near normal limits (Fig. 2A). P42 showed abnormally increased AF intensity in combination with nearly normal mean run-length distributed across the parapapillary region and the surrounding area (Fig. 2B). P47 and P34, in contrast, showed normal or nearly normal intensity distributions associated with biphasic run-length plots, showing normal results in a parapapillary region surrounded by an abnormally reduced run-length at greater eccentricities both in temporal and nasal retinas (Figs. 2C, 2D). It is important to note that regions of atrophy (such as in Fig. 2D) were masked (see Appendix) and did not contribute to the pseudoprofile results.

Patients with *ABCA4*-RD patients were divided into two groups: those with normal AF intensity pseudoprofiles within

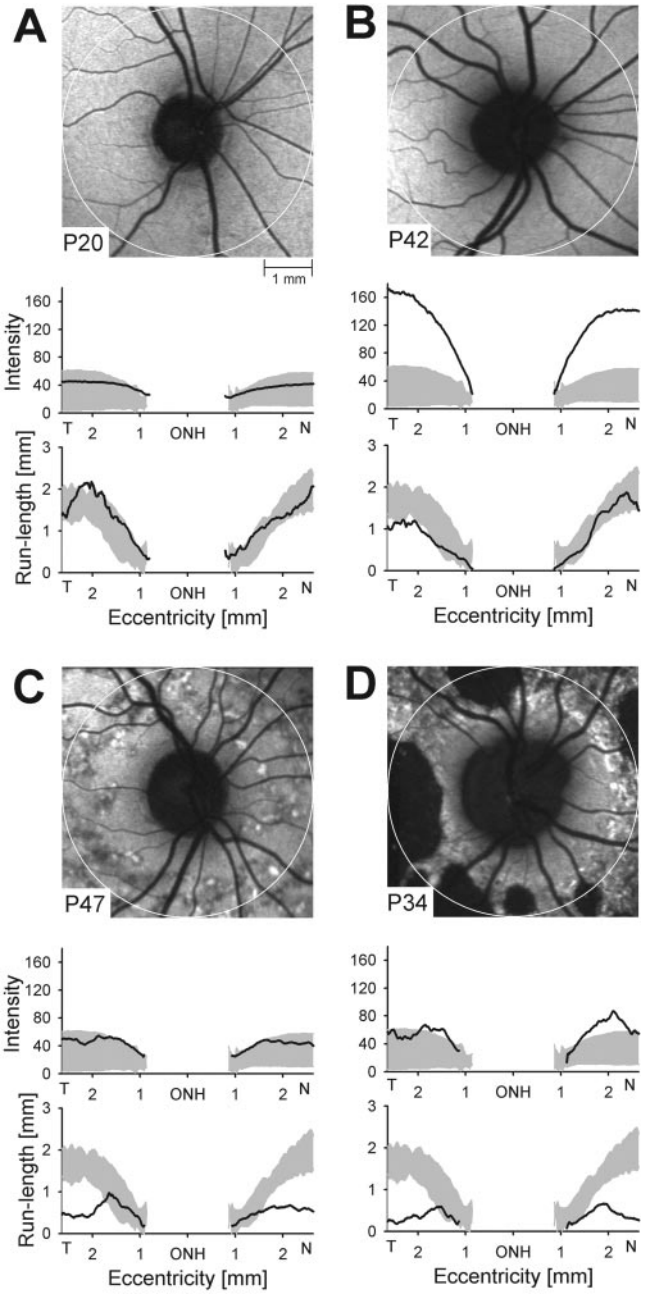

FIGURE 2. Detailed analysis of AF abnormalities in a region around the ONH in *ABCA4*-RD patients P20 (**A**), P42 (**B**), P47 (**C**), and P34 (**D**). The contrast of each grayscale image is uniformly stretched for better visibility of features. Standardized image data from temporal (T) and nasal (N) semiannular retinal regions from the edge of the ONH to an eccentricity of 2.5 mm (*white* circles overlaying the images) were analyzed and shown as pseudoprofiles of intensity and run-length. *Black lines*: data from patients; *shaded regions*: normal range.

or surrounding the parapapillary region (Fig. 3A, left panel) and those with abnormal results (Fig. 3A, right panel). The abnormalities were temporal to the ONH, nasal to the ONH, or both. Mean run-length pseudoprofiles ranged from normal to abnormal in both groups (Fig. 3B). Run-length abnormalities were dominated by numbers *smaller* than the mean normal values, implying an *increase* in local heterogeneity of AF intensities consistent with that visually appreciated from the images. The extent of run-length abnormality increased as a function of distance from the center of the ONH (Fig. 3B). Similarly, the percentage of patients showing normal run-length decreased as

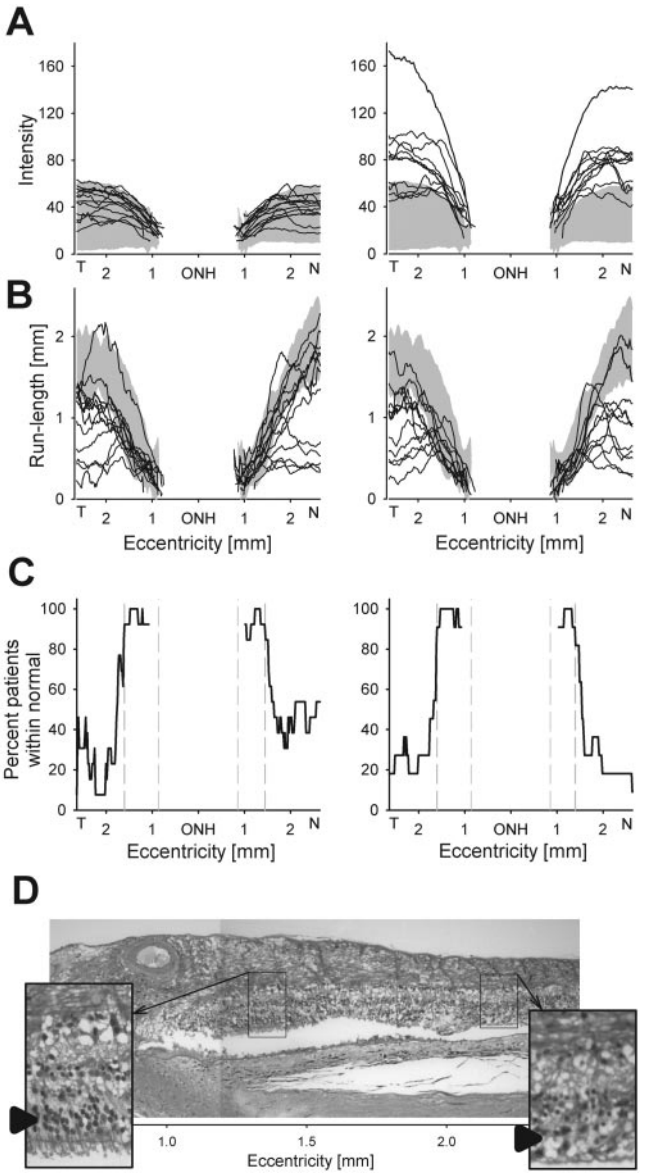

FIGURE 3. Quantification of the extent of parapapillary preservation in patients with *ABCA4*-RD. (**A**) Pseudoprofiles in the group of patients (*left*) showing normal AF intensity in the vicinity of the parapapillary region versus the remaining patients (*right*) showing abnormal results. (**B**) Pseudoprofiles of mean run-length in the same two groups of patients as shown in (**A**). (**C**) The percentage of patients in each group showing normal run-length results as a function of eccentricity from the center of the optic nerve. *Vertical dashed lines*: extents of parapapillary preservation defined as the eccentricity at which 90% of the patients show normal run-length. (**D**) Histopathology in a donor eye with Stargardt disease, showing the parapapillary region nasal to the ONH. *Insets*: the two *boxed* regions shown at higher magnification. *Arrowheads*: photoreceptor nuclei, which are more numerous in the parapapillary region.

a function of distance from the ONH (Fig. 3C). With 90% used as the criterion, the region of preserved parapapillary retina extended to 1.5–1.6 mm from the center of the ONH, corresponding to a ~0.6 mm (~2°) wide annular region (Fig. 3C, dashed lines) spared from the structural alterations of the RPE typically visible on AF imaging of patients with *ABCA4*-RD.

Histopathology results from a donor eye with STGD[34] (but without a known molecular diagnosis) allowed examination of retinal consequences of parapapillary sparing of the RPE, as visible on AF images. In the STGD eye, a zone immediately nasal to the ONH showed three to four rows of retained photoreceptor nuclei, with some inner segments and some very short outer segments (Fig. 3D). At further eccentricities, there was greater disease in the photoreceptor layer, which overlayed disorganized or absent RPE. The zone of relatively spared retina extended ~0.7 mm from the nasal edge of the ONH and thus appeared to correspond to the RPE preservation observed with AF imaging methods.

To evaluate the visual consequences of a structurally spared parapapillary region, we first considered psychophysical thresholds obtained in the central retinas of a subset of patients (8/41 = 19.5%) with documented foveal fixation. Most of these patients showed parafoveal losses of cone sensitivity with foveal thresholds either within the normal range or mildly reduced (Fig. 4A). Differences in the depth and extent of the parafoveal defects represented the severity of the central retinal disease in these patients. Unexpected was the apparent asymmetry of the visual function defect between the nasal and temporal paramacular retinas. For example, at 3-mm (10°) eccentricity, mean L/M cone sensitivity was significantly better (mean difference, 0.69 log; Student's *t*-test, $P = 0.05$) in the nasal retina near the ONH than in the temporal retina (Fig. 4A).

In patients with *ABCA4*-RD who had central scotomas, the preferred retinal locus of fixation was eccentric, as expected (Fig. 4B). Nineteen (46%) patients had a fixation locus in the superior retina. Ten patients (24% of all patients in the study, 30% of the subset of patients with central scotomas) demonstrated reproducible fixation loci in the parapapillary region (Fig. 4B). Six of these patients (P9, P18, P22, P33, P35, and P45) used the temporal parapapillary retina as the locus of fixation, placing their vision between the central scotoma caused by the *ABCA4* disease and the physiological blind spot caused by the ONH. Some patients fixated using parapapillary loci in both eyes when tested unilaterally (Fig. 4C).

We evaluated the relationship between a rank based measure of retina-wide disease severity (0 = least severe, 100 = most severe)[16] and the location of fixation. Eyes with foveal fixation showed the least disease severity (mean ± STD = 16.6 ± 14.5). Eyes with superior retinal fixation showed intermediate severity (38.3 ± 18.3), and eyes with parapapillary fixation were more severely affected (82.3 ± 10.1). Patients P30 and P38 were among the most severely affected (94.5 ± 4.9), and they showed fixations in the far superonasal and temporal retinal loci, respectively (Fig. 4B).

DISCUSSION

ABCA4-RD is generally accepted as showing a centrifugal gradient of disease severity with macular photoreceptors and RPE having greater vulnerability to dysfunction and cell loss compared with peripheral retina. The present study documented and explored a common and consistent exception to this presumed centrifugal gradient. The parapapillary retina and RPE are spared from degeneration, even at advanced disease stages. This spared region is also shown to be important for visual function in severely affected patients with central scotomas. We offer several hypotheses which, alone or in concert, may help explain these findings.

The *disc membrane–load hypothesis* could be invoked. This hypothesis suggests that a change in the photoreceptor to RPE ratio near the ONH explains parapapillary sparing. It is reasonable to assume that the local rate of lipofuscin accumulation is related to the local ratio of photoreceptors per RPE cell, based on the distribution of lipofuscin and AF intensity in normal subjects corresponding to the spatial density of rod photoreceptors,[35,36,39,41] and lipofuscin being derived from ingestion of photoreceptor outer segments.[40] Of interest, the parapapillary region in normal subjects shows a ring of decreased AF intensity[41] (Figs. 1, 2, 3), and the extent and shape

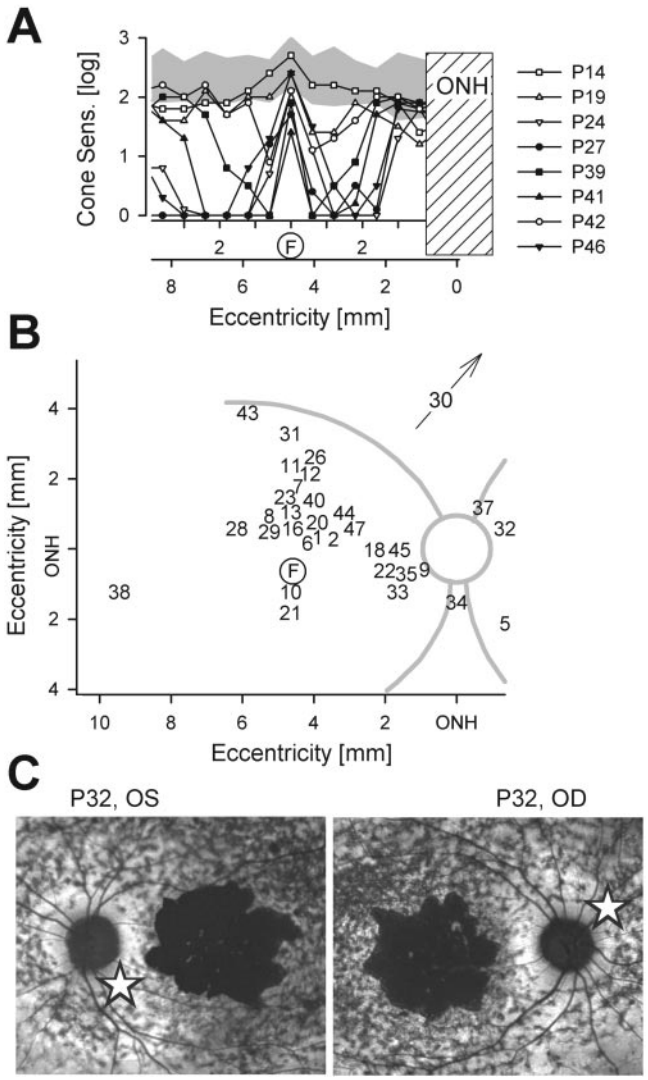

FIGURE 4. Visual function consequences of the preservation of parapapillary retina in *ABCA4* disease. (**A**) Psychophysical cone sensitivity profiles in patients with *ABCA4*-RD with documented foveal fixation. *Two horizontal axes*: the standard perimetric coordinate system centered on the fovea (F) and an alternate coordinate system centered on the ONH. *Hatched region*: expected location of the ONH; *shaded region*: normal range of cone sensitivity. (**B**) Retinal fixation loci in one eye of all patients (designated by numbers) with central scotomas and extrafoveal fixation. Data are shown as right-eye equivalent on a schematic showing the ONH (*circle*) and major retinal blood vessels (*curved lines*). *Arrow*: direction of fixation locus in P30 in the far superonasal retina. (**C**) AF images of both eyes of P32 with bilateral central atrophy of the RPE. *Stars*: fixation loci determined individually in each eye. The contrast of each grayscale image is uniformly stretched for better visibility of features.

of this ring is similar to the spared region in *ABCA4*-RD. A constitutively lower rate of lipofuscin accumulation in the normal parapapillary zone would be consistent with the dramatic decrease in photoreceptor density (from ~140,000 to ~65,000 cells/mm^2) that has been observed in this region of human eyes.[42] A reduced number of photoreceptors, together with an assumed invariant RPE density,[45] would relieve the disc membrane load of the parapapillary RPE cells and make them less vulnerable to the increase in lipofuscin accumulation[16] that occurs in *ABCA4*-RD. Inconsistent with this hypothesis is the local *reduction* in the photoreceptor-to-RPE cell ratio observed in the parafoveal region in primates,[46] a region that is extremely vulnerable to *ABCA4*-disease. Consistent with the disc membrane–load hypothesis is the dramatic reduction in photoreceptor density that normally occurs in the far peripheral retina,[42] where retinal histology was found to be unperturbed in a donor eye with STGD.[34]

The *light-load hypothesis* proposes that a local gradient in the penetration of light to the retina or the RPE underlies the finding. According to this hypothesis, parapapillary sparing occurs because of reduction of either lipofuscin accumulation[47] or photooxidative damage.[48,49] The retinal nerve fiber layer (RNFL) forms a prominent feature of the parapapillary retina, and light loss due to scattering[50] within the increasingly thicker RNFL may reduce the amount of light penetrating to the deeper layers. However, the topography of RFNL thickness is asymmetrically distributed around the ONH[51] and therefore is unlikely to be the principal cause of the circularly symmetric effect observed in the present study. An increase in retinal capillary vascularity has been observed at the parapapillary region of the monkey[52] but detailed topography of this effect is unknown, and the correspondence to the spared parapapillary ring cannot be determined at this time. There could also be a parapapillary increase in melanin concentration protecting RPE cells from light-induced apoptosis[53]; however, use of infrared excitation to obtain AF images dominated by melanin have not shown telltale signs of a high-intensity ring surrounding the ONH to support such a speculation[54] (Keilhauer CN, et al. *IOVS* 2005;46:ARVO E-Abstract 1394; Weinberger AWA, et al. *IOVS* 2005;46:ARVO E-Abstract 2585).

The *lipofuscin-clearance hypothesis* favors increased removal of lipofuscin in the parapapillary region as a cause of the spared annulus in *ABCA4*-RD. The existence of a clearance mechanism for lipofuscin from RPE cells has been controversial.[47,55] If there were an effective mechanism of lipofuscin clearance in humans, local changes in choriocapillaris properties observed in the parapapillary region could affect the accumulation of this substance.[27,56]

The *neurotrophic factors hypothesis* suggests there may be increases in factors that enhance neuronal survival around the ONH. Consistent with this hypothesis, increased immunoreactivity for basic fibroblast growth factor (bFGF) has been observed around the edge of the ONH in normal mouse retinas.[57] Such a local gradient could provide protection to photoreceptors from degeneration, and this effect has been observed in some animal studies.[57–62] Of note, human retinas show a centrifugal gradient of bFGF immunoreactivity in rod nuclei[63]; however, the spatial topography of bFGF or other factors around the human ONH is currently unknown, and a causal relationship between increased neurotrophic factors and preserved parapapillary retina or RPE remains speculative.

Not all human retinopathies show sparing of the parapapillary region; some even show enhanced vulnerability of this region. Molecularly characterized retinal degenerations in the latter category include Sveinsson's chorioretinal atrophy caused by dominant mutations in the *TEAD1* gene,[64] some phenotypes of X-linked RP caused by *RP2* mutations,[65] and Malattia Leventinese/Doyne honeycomb retinal dystrophy caused by a mutation in *EFEMP1*.[66] Of interest, vulnerability of the parapapillary region is also seen in normal aging and in age-related macular disease[67–69] (Keilhauer CN, et al. *IOVS* 2004;45:ARVO E-Abstract 3078). Better understanding of the special properties of the parapapillary region may contribute to understanding of the molecular/cellular disease mechanisms involved in different retinal degenerative diseases with dramatically contrasting effects on this region.

The current work also has implications for further *ABCA4*-RD clinical studies. The region between the fovea and optic nerve, convenient and accessible for imaging and visual function measurements, may be informative of the entire gamut of *ABCA4* disease expression, from barely detectable disease at the parafovea at the earliest stages to still-detectable function in the parapapillary area at the most severe stages.

Tests of structure and function densely sampling this region may help determine natural history or outcome of therapy at all severity stages of *ABCA4*-RD.

APPENDIX

Run-Length Analysis

AF imaging studies in patients with retinal degenerative diseases have shown that not only the absolute intensity but also the local heterogeneity of the intensity correlates with the clinical impression of local disease severity.[28,44] We have recently quantified this heterogeneity in *ABCA4*-RD by calculating the local standard deviation of AF intensity at a midperipheral locus and have shown how an abnormal increase in this measure precedes localized changes in rod- and cone-mediated visual function.[16] In the current work, we used an alternative measure of "local" texture that is more appropriate for regions with local discontinuities (such as the parapapillary region) and also produces quantitative results in terms of retinal distances that are easier to interpret.

Many texture-analysis methods have been proposed based on the two major characteristics of images: coarseness and directionality.[31,32] The run-length analysis method combines statistical and structural approaches to image texture.[32] A primitive, called gray level run, is defined as the set of consecutive, collinear pixels having the same gray level. Image regions with heterogeneous intensity have shorter runs than regions with more homogeneous intensity.[33]

To quantify the local AF heterogeneity across the retina we calculated the mean run-length at each pixel (representative example shown in Fig. A1), by using two images: the AF intensity image and a mask image showing the location of major blood vessels, ONH, and regions of atrophy. The AF intensity image was spatially filtered with a Gaussian filter (radius, 5 pixels) to minimize the contribution of the noise produced by the avalanche photodiode detector. Run-lengths were calculated along the eight principal directions and averaged. Run-length at each pixel was defined as the pixel-to-pixel distance multiplied by the number of consecutive, collinear neighbors having an intensity within 10% of the pixel. A principal direction was not included in averaging if a pixel corresponding to a masked value or the edge of the frame was reached. Pixel-to-pixel distance was defined as 17.5 μm along the axes and 24.9 μm along the diagonals. The result of this texture analysis method is an image where the value of each pixel represents the mean radius of a circular region over which the AF intensity would be expected to be nearly homogeneous.

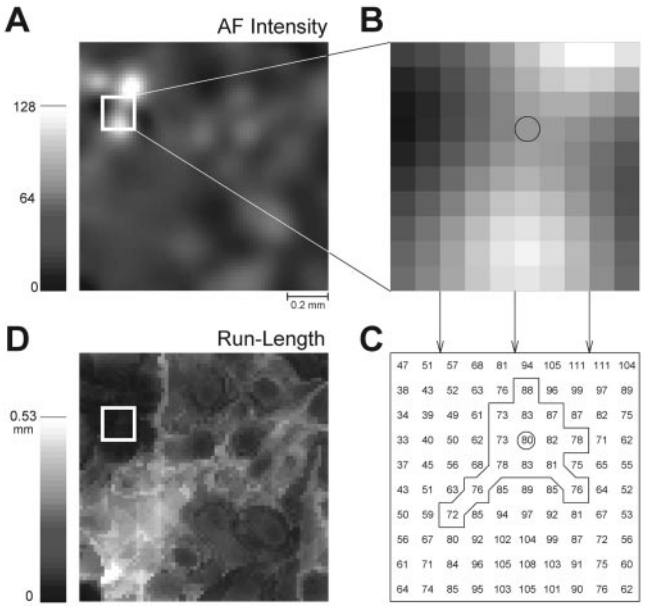

FIGURE A1. Estimation of local intensity heterogeneity by calculating the mean run-length image. (**A**) A representative AF intensity image showing regions of high local heterogeneity and of relative homogeneity. The contrast of the grayscale images are uniformly stretched for better visibility of features. (**B**) Magnification of a 10 × 10-pixel region of the image in (**A**). (**C**) Intensities corresponding to each pixel of the magnified grayscale image shown in (**B**). The extents of run-lengths in eight principal directions are demarcated (*lines*) around a chosen pixel of interest (*circle*); the mean run-length is 1.99 pixels, which corresponds to 0.035 mm on the retina. (**D**) Grayscale representation of the mean run-lengths calculated at each pixel for the image shown in (**A**). Regions of local intensity heterogeneity have short run-lengths and darker pixels, and regions of local intensity homogeneity have longer run-lengths and lighter pixels.

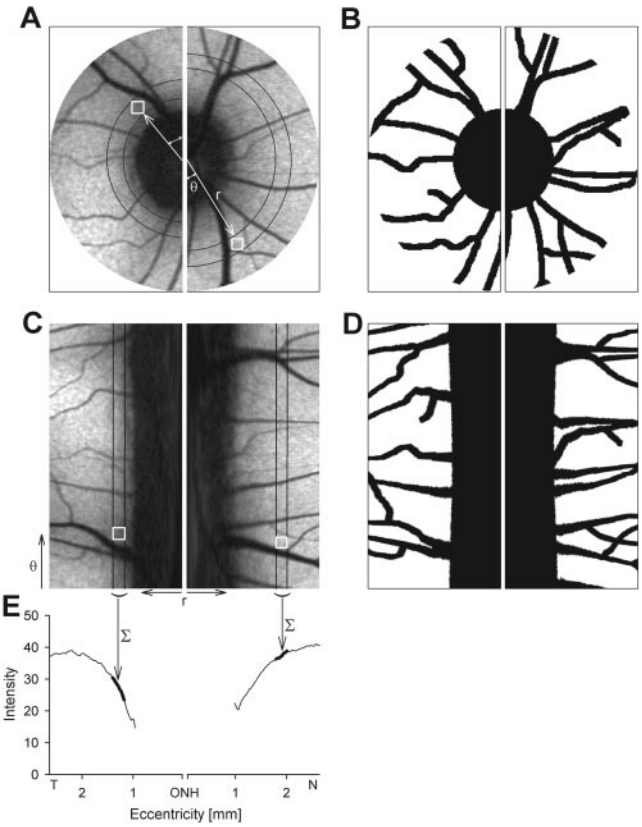

FIGURE A2. Demonstration of the semipolar integral transformation used to perform data reduction on images. (**A**) A representative AF intensity image of the parapapillary region is divided into temporal and nasal halves. Radius (r) and angle (θ) axes of polar coordinates are shown with respect to the center of the ONH. (**B**) A two-level masked image showing image pixels (*black*) corresponding to ONH and retinal blood vessels that are to be excluded from further calculations. (**C**, **D**) Application of a rectangular-to-polar transformation to the intensity and masked images shown in (**A**) and (**B**). Representative regions (*vertical lines*) and locations (*boxes*) demonstrating the correspondence between rectangular and polar coordinate representations are shown in (**A**) and (**C**). (**E**) The result of integrating the semipolar transformed images along the angle coordinate. Locations corresponding to black pixels of the masked image are not included in the integral.

Pseudoprofiles Derived from Semipolar Integral Analysis

Data reduction strategies applied to AF intensity and texture images could facilitate statistical comparison of results between patients. It would be preferable to attempt to retain an

intuitive link in the reduced data to the exquisite spatial information contained in the underlying images. In the current work, this link was achieved by taking advantage of the approximate circular symmetry of the parapapillary region.

To perform a semipolar integral analysis (representative example shown in Fig. A2), we used registered pairs of AF intensity (or texture) and masked images. First, a 300 × 300 pixel region of interest centered on the ONH was cropped and split vertically into temporal and nasal halves (Figs. A2A, A2B). Then, values of each pixel were sampled onto temporary images representing polar coordinates (Figs. A2C, A2D). Integration was performed along the angle coordinate excluding the masked pixels (i.e., those retinal regions corresponding to major blood vessels, ONH, and regions of atrophy). The result of the semipolar integral (Fig. A2E) is a pseudoprofile that has the intuitiveness of a profile across the ONH but includes quantitative data from all the parapapillary annulus.

Acknowledgments

The authors thank Elaine Smilko, Elizabeth Windsor, Alejandro Roman, Elaine DeCastro, Leigh Gardner, Jessica Emmons, Jiancheng Huang, William Nyberg, and John Chico for their assistance during the project and Marco Zarbin for valuable ideas that contributed to the work.

References

1. Papermaster DS, Reilly P, Schneider BG. Cone lamellae and red and green rod outer segment disks contain a large intrinsic membrane protein on their margins: an ultrastructural immunocytochemical study of frog retinas. *Vision Res*. 1982;22:1417–1428.
2. Allikmets R, Singh N, Sun H, et al. A photoreceptor cell-specific ATP-binding transporter gene (ABCR) is mutated in recessive Stargardt macular dystrophy. *Nat Genet*. 1997;15:236–246.
3. Azarian SM, Travis GH. The photoreceptor rim protein is an ABC transporter encoded by the gene for recessive Stargardt's disease (ABCR). *FEBS Letts*. 1997;409:247–252.
4. Sun H, Nathans JR. Stargardt's ABCR is localized to the disc membrane of the retinal rod outer segments. *Nat Genet*. 1997;17:15–16.
5. Molday LL, Rabin AR, Molday RS. ABCR expression in foveal cone photoreceptors and its role in Stargardt macular dystrophy. *Nat Genet*. 2000;25:257–258.
6. Weng J, Mata NL, Azarian SM, Tzekov RT, Birch DG, Travis GH. Insights into the function of rim protein in photoreceptors and etiology of Stargardt's disease from the phenotype in ABCR knockout mice. *Cell*. 1999;98:13–23.
7. Sun H, Molday RS, Nathans J. Retinal stimulates ATP hydrolysis by purified and reconstituted ABCR, the photoreceptor-specific ATP-binding cassette transporter responsible for Stargardt disease. *J Biol Chem*. 1999;274:8269–8281.
8. Beharry S, Zhong M, Molday RS. N-retinylidene-phosphatidylethanolamine is the preferred retinoid substrate for the photoreceptor-specific ABC transporter ABCA4 (ABCR). *J Biol Chem*. 2004;279:53972–53979.
9. Martinez-Mir A, Paloma E, Allikmets R, et al. Retinitis pigmentosa caused by a homozygous mutation in the Stargardt disease gene ABCR. *Nat Genet*. 1998;18:11–12.
10. Cremers FPM, van de Pol DJR, van Driel M, et al. Autosomal recessive retinitis pigmentosa and cone-rod dystrophy caused by splice site mutations in the Stargardt's disease gene ABCR. *Hum Mol Genet*. 1998;7:355–362.
11. Fishman GA, Stone EM, Grover S, Derlacki DJ, Haines HL, Hockney RR. Variation of clinical expression in patients with Stargardt dystrophy and sequence variations in the ABCR gene. *Arch Ophthalmol*. 1999;117:504–510.
12. Webster AR, Heon E, Lotery AJ, et al. An analysis of allelic variation in the ABCA4 gene. *Invest Ophthalmol Vis Sci*. 2001;42:1179–1189.
13. Birch DG, Peters AY, Locke KL, Spencer R, Megarity CF, Travis GH. Visual function in patients with cone-rod dystrophy (CRD) associated with mutations in the ABCA4(ABCR) gene. *Exp Eye Res*. 2001;73:877–886.
14. Gerth C, Andrassi-Darida M, Bock M, Preising MN, Weber BH, Lorenz B. Phenotypes of 16 Stargardt macular dystrophy/fundus flavimaculatus patients with known ABCA4 mutations and evaluation of genotype-phenotype correlation. *Graefes Arch Clin Exp Ophthalmol*. 2002;240:628–638.
15. Fishman GA, Stone EM, Eliason DA, Taylor CM, Lindeman M, Derlacki DJ. ABCA4 gene sequence variations in patients with autosomal recessive cone-rod dystrophy. *Arch Ophthalmol*. 2003;121:851–855.
16. Cideciyan AV, Aleman TS, Swider M, et al. Mutations in ABCA4 result in accumulation of lipofuscin before slowing of the retinoid cycle: a reappraisal of the human disease sequence. *Hum Mol Genet*. 2004;13:525–534.
17. Klevering BJ, Deutman AF, Maugeri A, Cremers FP, Hoyng CB. The spectrum of retinal phenotypes caused by mutations in the ABCA4 gene. *Graefes Arch Clin Exp Ophthalmol*. 2005;243:90–100.
18. Aaberg TM. Stargardt's disease and fundus flavimaculatus: evaluation of morphologic progression and intrafamilial co-existence. *Trans Am Ophthalmol Soc*. 1986;84:453–487.
19. Aaberg TM, Han DP. Evaluation of phenotypic similarities between Stargardt flavimaculatus and retinal pigment epithelial pattern dystrophies. *Trans Am Ophthalmol Soc*. 1987;85:101–119.
20. Armstrong JD, Meyer D, Xu S, Elfervig JL. Long-term follow-up of Stargardt's disease and fundus flavimaculatus. *Ophthalmology*. 1998;105:448–457.
21. Rotenstreich Y, Fishman GA, Anderson RJ. Visual acuity loss and clinical observations in a large series of patients with Stargardt disease. *Ophthalmology*. 2003;110:1151–1158.
22. Passmore JA, Robertson DM. Ring scotomata in fundus flavimaculatus. *Am J Ophthalmol*. 1975;80:907–912.
23. Weiter JJ, Delori F, Dorey CK. Central sparing in annular macular degeneration. *Am J Ophthalmol*. 1988;106:286–292.
24. Klein R, Lewis RA, Meyers SM, Myers FL. Subretinal neovascularization associated with fundus flavimaculatus. *Arch Ophthalmol*. 1978;96:2054–2057.
25. De Laey JJ, Verougstraete C. Hyperlipofuscinosis and subretinal fibrosis in Stargardt's disease. *Retina*. 1995;15:399–406.
26. Wroblewski JJ, Gitter KA, Cohen G, Schomaker K. Indocyanine green angiography in Stargardt's flavimaculatus. *Am J Ophthalmol*. 1995;120:208–218.
27. Schwoerer J, Secretan M, Zografos L, Piguet B. Indocyanine green angiography in Fundus flavimaculatus. *Ophthalmologica*. 2000;214:240–245.
28. Lois N, Halfyard AS, Bird AC, Holder GE, Fitzke FW. Fundus autofluorescence in Stargardt macular dystrophy-fundus flavimaculatus. *Am J Ophthalmol*. 2004;138:55–63.
29. Jacobson SG, Voigt WJ, Parel J-M, et al. Automated light- and dark-adapted perimetry for evaluating retinitis pigmentosa. *Ophthalmology*. 1986;93:1604–1611.
30. Thévenaz P, Ruttimann UE, Unser M. A pyramid approach to subpixel registration based on intensity. *IEEE Trans Image Proc*. 1998;7:27–41.
31. Haralick RM, Dinstein I, Shanmugam K. Textural features for image classification. *IEEE Trans Syst Man Cybern*. 1973;3:610–621.
32. Galloway MM. Texture analysis using gray level run-lengths. *Comput Graphics Image Proc*. 1975;4:172–179.
33. Herlidou S, Grebe R, Grados F, Leuyer N, Fardellone P, Meyer ME. Influence of age and osteoporosis on calcaneus trabecular bone structure: a preliminary in vivo MRI study by quantitative texture analysis. *Magn Reson Imaging*. 2004;22:237–243.
34. Birnbach CD, Järveläinen M, Possin DE, Milam AH. Histopathology and immunocyto-chemistry of the neurosensory retina in fundus flavimaculatus. *Ophthalmology*. 1994;101:1211–1219.
35. Wing GL, Blanchard GC, Weiter JJ. The topography and age relationship of lipofuscin concentration in the retinal pigment epithelium. *Invest Ophthalmol Vis Sci*. 1978;17:601–607.
36. Weiter JJ, Delori FC, Wing G, Fitch KA. Retinal pigment epithelial lipofuscin and melanin and choroidal melanin in human eyes. *Invest Ophthalmol Vis Sci*. 1986;27:145–152.
37. Eldred GE, Katz ML. Fluorophores of the human retinal pigment epithelium: separation and spectral characterization. *Exp Eye Res*. 1988;47:71–86.
38. Delori FC, Dorey CK, Staurenghi G, Arend O, Goger DG, Weiter JJ. In vivo fluorescence of the ocular fundus exhibits retinal pig-

ment epithelium lipofuscin characteristics. *Invest Ophthalmol Vis Sci*. 1995;36:718–729.

39. von Ruckmann A, Fitzke FW, Bird AC. Distribution of fundus autofluorescence with a scanning laser ophthalmoscope. *Br J Ophthalmol*. 1995;79:407–412.
40. Sparrow JR, Fishkin N, Zhou J, et al. A2E, a byproduct of the visual cycle. *Vision Res*. 2003;43:2983–2990.
41. Delori FC, Goger DG, Dorey CK. Age-related accumulation and spatial distribution of lipofuscin in RPE of normal subjects. *Invest Ophthalmol Vis Sci*. 2001;42:1855–1866.
42. Curcio CA, Sloan KR, Kalina RE, Hendrickson AE. Human photoreceptor topography. *J Comp Neurol*. 1990;292:497–523.
43. Delori FC, Staurenghi G, Arend O, Dorey CK, Goger DG, Weiter JJ. In vivo measurement of lipofuscin in Stargardt's disease-fundus flavimaculatus. *Invest Ophthalmol Vis Sci*. 1995;36:2327–2331.
44. von Ruckmann A, Fitzke FW, Bird AC. In vivo fundus autofluorescence in macular dystrophies. *Arch Ophthalmol*. 1997;115:609–615.
45. Del Priore LV, Kuo YH, Tezel TH. Age-related changes in human RPE cell density and apoptosis proportion in situ. *Invest Ophthalmol Vis Sci*. 2002;43:3312–3318.
46. Snodderly DM, Sandstrom MM, Leung IY, Zucker CL, Neuringer M. Retinal pigment epithelial cell distribution in central retina of rhesus monkeys. *Invest Ophthalmol Vis Sci*. 2002;43:2815–2818.
47. Mata NL, Weng J, Travis GH. Biosynthesis of a major lipofuscin fluorophore in mice and humans with ABCR-mediated retinal and macular degeneration. *Proc Natl Acad Sci USA*. 2000;97:7154–7259.
48. Sparrow JR, Nakanishi K, Parish CA. The lipofuscin fluorophore A2E mediates blue light-induced damage to retinal pigmented epithelial cells. *Invest Ophthalmol Vis Sci*. 2000;41:1981–1989.
49. Schutt F, Davies S, Kopitz J, Holz FG, Boulton ME. Photodamage to human RPE cells by A2-E, a retinoid component of lipofuscin. *Invest Ophthalmol Vis Sci*. 2000;41:2303–2308.
50. Knighton RW, Jacobson SG, Kemp CM. The spectral reflectance of the nerve fiber layer of the macaque retina. *Invest Ophthalmol Vis Sci*. 1989;30:2392–2402.
51. Frenkel S, Morgan JE, Blumenthal EZ. Histological measurement of retinal nerve fibre layer thickness. *Eye*. 2005;19:491–498.
52. Snodderly DM, Weinhaus RS, Choi JC. Neural-vascular relationships in central retina of macaque monkeys (Macaca fascicularis). *J Neurosci*. 1992;12:1169–1193.
53. Seagle BL, Rezai KA, Kobori Y, Gasyna EM, Rezaei KA, Norris JR Jr. Melanin photoprotection in the human retinal pigment epithelium and its correlation with light-induced cell apoptosis. *Proc Natl Acad Sci USA*. 2005;102:8978–8983.
54. Piccolino FC, Borgia L, Zinicola E, Iester M, Torrielli S. Pre-injection fluorescence in indocyanine green angiography. *Ophthalmology*. 1996;103:1837–1845.
55. Katz ML. Potential reversibility of lipofuscin accumulation. *Arch Gerontol Geriatr*. 2002;34:311–317.
56. Hayreh SS. Blood flow in the optic nerve head and factors that may influence it. *Prog Retin Eye Res*. 2001;20:595–624.
57. Stone J, Maslim J, Valter-Kocsi K, et al. Mechanisms of photoreceptor death and survival in mammalian retina. *Prog Retin Eye Res*. 1999;18:689–735.
58. LaVail MM, Battelle BA. Influence of eye pigmentation and light deprivation on inherited retinal dystrophy in the rat. *Exp Eye Res*. 1975;21:167–192.
59. Lawwill T, Crockett S, Currier G. Retinal damage secondary to chronic light exposure, thresholds and mechanisms. *Doc Ophthalmol*. 1977;44:379–402.
60. Noell WK. Possible mechanisms of photoreceptor damage by light in mammalian eyes. *Vision Res*. 1980;20:1163–1171.
61. Tso MO, Woodford BJ. Effect of photic injury on the retinal tissues. *Ophthalmology*. 1983;90:952–963.
62. Wang T, Milam AH, Steel G, Valle D. A mouse model of gyrate atrophy of the choroid and retina. Early retinal pigment epithelium damage and progressive retinal degeneration. *J Clin Invest*. 1996;97:2753–2762.
63. Li ZY, Chang JH, Milam AH. A gradient of basic fibroblast growth factor in rod photoreceptors in the normal human retina. *Vis Neurosci*. 1997;14:671–679.
64. Fossdal R, Jonasson F, Kristjansdottir GT, et al. A novel TEAD1 mutation is the causative allele in Sveinsson's chorioretinal atrophy (helicoid peripapillary chorioretinal degeneration). *Hum Mol Genet*. 2004;13:975–981.
65. Dandekar SS, Ebenezer ND, Grayson C, et al. An atypical phenotype of macular and peripapillary retinal atrophy caused by a mutation in the RP2 gene. *Br J Ophthalmol*. 2004;88:528–532.
66. Haimovici R, Wroblewski J, Piguet B, et al. Symptomatic abnormalities of dark adaptation in patients with EFEMP1 retinal dystrophy (Malattia Leventinese/Doyne honeycomb retinal dystrophy). *Eye*. 2002;16:7–15.
67. Sunness JS, Bressler NM, Tian Y, Alexander J, Applegate CA. Measuring geographic atrophy in advanced age-related macular degeneration. *Invest Ophthalmol Vis Sci*. 1999;40:1761–1769.
68. Curcio CA, Saunders PL, Younger PW, Malek G. Peripapillary chorioretinal atrophy: Bruch's membrane changes and photoreceptor loss. *Ophthalmology*. 2000;107:334–343.
69. Chong NH, Keonin J, Luthert PJ, et al. Decreased thickness and integrity of the macular elastic layer of Bruch's membrane correspond to the distribution of lesions associated with age-related macular degeneration. *Am J Pathol*. 2005;166:241–251.